Finite Element Solution to Groundwater Transport of Solutes Undergoing Decay and Non-Linear Sorption

Domenico Baú
Department of Civil & Environmental Engineering
Colorado State University, Fort Collins, CO, 80523, USA
E-mail: domenico.bau@colostate.edu

1 Introduction

Contaminants are often found in groundwater as a result of disposal or leakage of urban sewage and industrial wastes, surficial applications of pesticides and fertilizers used in agriculture, atmospheric deposition or accidental releases of chemicals on the ground surface. Contamination can originate from point sources or nonpoint sources. Typical contaminants are organic compounds, trace metals, and radionuclides. Once contaminants enter the subsurface, they may reach shallow aquifers, where they dissolve in water, and are transported downstream along flow pathways. Dissolved pollutants may thus contaminate withdrawal sites at pumping wells, or reappear at the surface, thus posing serious risks for human health or ecosystems in general.

Contaminants dissolved in groundwater typically experience complex physical and chemical processes such as advection, diffusion, chemical reactions, sorption, biodegradation and decay. Understanding and simulating these processes is crucial to predict the fate and transport of solutes in groundwater. However, the study of contaminant transport is often hindered by the limited ability to sufficiently characterize the inherent heterogeneities and anisotropies in the subsurface, the reaction pathways of chemical processes and the time scales at which they occur.

Mathematical models of groundwater flow and reactive transport may provide an effective tool to study these processes when supported by consistent and reliable datasets. These models rely on the fundamental equations of mass conservation for the aquifer/contaminant system and describe the migration and the fate of contaminants in groundwater. Because of their complexity, analytical solutions to these differential equations are available only for highly simplified, ideal settings. Numerical approaches are thus necessary to realistically represent real-world scenarios.

In this work, a two-dimensional finite-element simulation model is presented that solves the contaminant transport equation for a solute undergoing advection, dispersion, first-order decay, and non-linear local-equilibrium sorption. Sorption onto solid grains is one the most important processes affecting the fate of contaminants dissolved in groundwater. In those instances where sorption rates are much faster than the rates of advection and dispersion, one may reasonably assume conditions of "local equilibrium", in which the sorbed phase achieves instantaneous equilibrium with the dissolved phase. The relationships that link

sorbed concentrations to solute concentration are called "sorption isotherms" [3]. Sorption is said to be non-linear when these isotherms are non-linear functions. Non-linear sorption introduces a source of non linearity in the transport partial differential equation. Detailed reviews of sorption models may be found in Brusseau and Rao [2], Weber Jr. *et al.* [15].

The contaminant transport model presented in this work extends the numerical model "TRAN2D" of Gambolati *et al.* [6] to dealing with non-linear sorption isotherms. In this numerical model, called "TRAN2D.NLS", the non linearity is tackled using a direct iterative approach based upon a Picard linearization. This method is implemented using several types of sorption isotherms, which can be specified arbitrarily in however heterogeneous settings.

2 Mathematical Model for Transport Under Equilibrium Conditions

The equation describing the transport in variably saturated porous media of contaminants undergoing first-order radioactive (or biodegradation) decay and local equilibrium sorption may be written as [1, 11, 5, 6]:

$$\begin{aligned}&\frac{\partial}{\partial x_i}\left(D_{ij}\cdot\frac{\partial c}{\partial x_j}\right)-\frac{\partial}{\partial x_i}(v_i\cdot c)-n\cdot S_w\cdot\lambda c-\rho_b\cdot\lambda\cdot S=\\&=\frac{\partial(n\cdot S_w\cdot c)}{\partial t}+\rho_b\cdot\frac{\partial S}{\partial t}-q\cdot c^*-f\end{aligned}\tag{1}$$

where: x_i is the ith Cartesian coordinate ($i=1,2$); t is time [T]; n is the porosity of the medium [/]; S_w is the water saturation [/]; v_i is the Darcy velocity [L/T]; D_{ij} is the dispersion tensor [L^2/T]; c is the concentration of the dissolved constituent [M/L^3]; q represents distributed source or sink terms (volumetric flow rate per unit volume) [T^{-1}]; c^* is the concentration of the solute injected or withdrawn with the fluid source or sink [M/L^3]; λ is the rate constant of decay [1/T]; S is the concentration of the adsorbed constituent in the solid phase [M/M]; $\rho_b=(1-n)\cdot\rho_s$ is the bulk density [M/L^3]; ρ_s is the solid density [M/L^3]; and f is the distributed mass rate of the solute per unit volume [M/L^3T].

In Equation (1), the dispersion tensor is given by [1]:

$$D_{ij}=n\cdot S_w\cdot\tilde{D}_{ij}=(\alpha_T\cdot\mid v\mid+n\cdot S_w\cdot D_0\cdot\tau)\cdot\delta_{ij}+(\alpha_L-\alpha_T)\cdot\frac{v_i\cdot v_j}{\mid v\mid}\tag{2}$$

where: $i,j=1,2$; $\mid v\mid=\sqrt{v_1^2+v_2^2}$; α_L is the longitudinal dispersivity [L]; α_T is the transversal dispersivity [L]; δ_{ij} is the Kronecker delta [/]; D_o is the molecular diffusion coefficient [L^2/T]; τ is the tortuosity [/].

Equation (1) may be expanded by applying the "chain rule" to the advective term:

$$\begin{aligned}&\frac{\partial}{\partial x_i}\left(D_{ij}\cdot\frac{\partial c}{\partial x_j}\right)-v_i\cdot\frac{\partial c}{\partial x_i}-c\cdot\frac{\partial v_i}{\partial x_i}-n\cdot S_w\cdot\lambda c-\rho_b\cdot\lambda\cdot S=\\&=\frac{\partial(n\cdot S_w\cdot c)}{\partial t}+\rho_b\cdot\frac{\partial S}{\partial t}-qc^*-f\end{aligned}\tag{3}$$

From Richards' Equation [13], which governs flow in variably saturated porous media:

$$\frac{\partial v_i}{\partial x_i}=q-\frac{\partial(n\cdot S_w)}{\partial t}\tag{4}$$

After substitution of Equation (4) into Equation (3), the latter becomes:

$$\begin{aligned} \frac{\partial}{\partial x_i}\left(D_{ij}\cdot\frac{\partial c}{\partial x_j}\right) - v_i\cdot\frac{\partial c}{\partial x_i} &= n\cdot S_w\cdot\left(\frac{\partial c}{\partial t}+\lambda\cdot c\right)+ \\ &+ \rho_b\cdot\left(\frac{\partial S}{\partial t}+\lambda\cdot S\right)+q\cdot(c-c^*)-f \end{aligned} \tag{5}$$

It is worth to observe that if q denotes a sink term then $c = c^*$ and the term $q(c-c^*)$ vanishes.

The initial and boundary conditions for the transport Equation (5) can be expressed as [4]:

$$c(x_i,0) = c_o(x_i) \tag{6a}$$

$$c(x_i,t) = \overline{c}(x_i,t) \qquad \text{on } \Gamma_D \tag{6b}$$

$$D_{ij}\cdot\frac{\partial c}{\partial x_j}\cdot n_i = q_c^N(x_i,t) \qquad \text{on } \Gamma_N \tag{6c}$$

$$\left(D_{ij}\cdot\frac{\partial c}{\partial x_j} - v_i\cdot c\right)\cdot n_i = q_c^C(x_i,t) \qquad \text{on } \Gamma_C \tag{6d}$$

where: c_o is the initial concentration; $\overline{c}$ is the prescribed concentration on the Dirichlet boundary Γ_D; q_c^N is the prescribed dispersive flux normal to the Neumann boundary Γ_N (positive outwards); and q_c^C is the prescribed total flux of solute across the Cauchy or Rubin boundary Γ_C.

3 Sorption isotherms

Sorption is typically estimated experimentally by measuring the solute concentration sorbed on a particular sediment, soil, or rock type. It is observed that the sorption capacity is generally a function of the solute concentration in the aqueous phase [2, 15]. Such a function is called "sorption isotherm". If sorption is much faster than the fluid velocity, then the solute may be considered locally in a condition of constant equilibrium with the sorbed phase. Equilibrium sorption isotherms are known to depend on several factors, such as surface charge of the sorbing phase, ionic strength, solution pH, competing counter-ions and their concentrations, and the concentration of the sorbed phase. In some cases the "adsorption" isotherm may be different from the "desorption" isotherm (chemical hysteresis) [3].

In the numerical approach presented here, the equilibrium sorption isotherm is expressed as a generic function:

$$S = S(c) \tag{7}$$

Examples of sorption models that may be dealt with are the Freundlich isotherm and the Langmuir isotherm [3]. The Freundlich sorption isotherm is defined by:

$$S = S(c) = K_F\cdot c^N \tag{8}$$

where: K_F is referred to as the distribution coefficient $[(\mathrm{L}^3/\mathrm{M})^N]$, and N is a constant.

Examples of Freundlich isotherms are shown in Figure 1. If N is equal to 1, a linear sorption isotherm is obtained. Since with Freundlich isotherms no upper bound to the sorbed concentration may be accounted for, their use should be restricted within the concentration limits of experimental data.

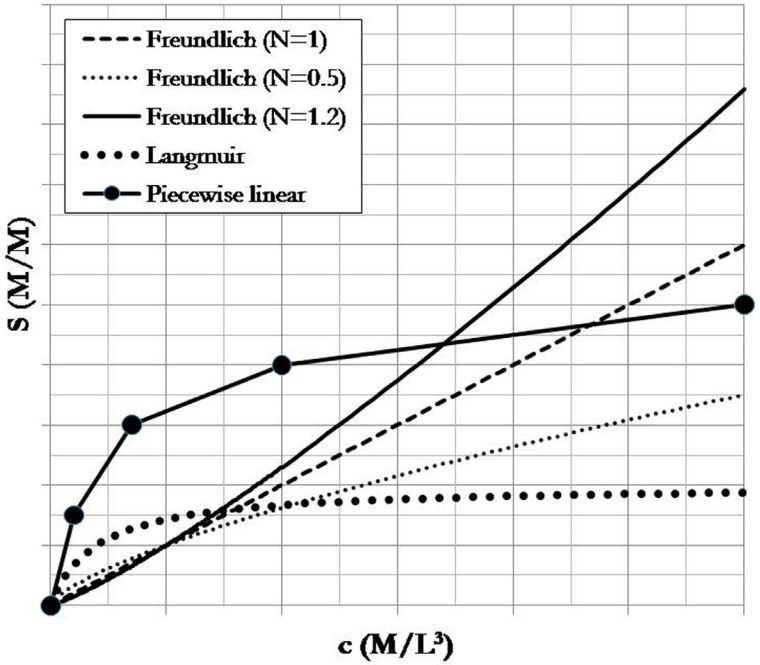

Figure 1: Sorption isotherm models implemented in TRAN2D.NLS.

The Langmuir isotherm was developed to limit the sorbed concentration to the maximum amount of solute that can be sorbed onto the solid phase. This isotherm can be expressed as:

$$S = S\left(c\right) = \frac{S_{lim} \cdot K_L \cdot c}{S_{lim} + K_L \cdot c} \tag{9}$$

where: K_L is an adsorption constant, which depends on the binding energy [L^3/M]; S_{lim} is the sorption capacity [M/M].

Figure 1 shows examples of the sorption isotherms that may be prescribed in TRAN2D.NLS. The model also allows for generalizing the sorption isotherm by including a piecewise linear function (see Figure 1), which may be fitted to any set of experimental data.

4 Finite-Element Solution

The substitution of Equation (7) into Equation (5) gives:

$$\frac{\partial}{\partial x_i}\left(D_{ij} \cdot \frac{\partial c}{\partial x_j}\right) - v_i \cdot \frac{\partial c}{\partial x_i} = n \cdot S_w \cdot \left(\frac{\partial c}{\partial t} + \lambda \cdot c\right) +$$
$$+\rho_b \cdot \left[\frac{dS}{dc} \cdot \frac{\partial c}{\partial t} + \lambda \cdot S\left(c\right)\right] + q \cdot \left(c - c^*\right) - f \tag{10}$$

Equation (10) is non-linear since S depends upon c through Equation (7). The finite-element integration of the transport Equation (10) relies upon an approximate solution given in the form of a linear combination of N_n linear basis functions $N_g(x_1, x_2)$ for two-dimensional triangular finite elements:

$$c \approx \hat{c} = \sum_{g=1}^{N_n} N_g(x_1, x_2) \cdot c_g(t) \tag{11}$$

where $c_g(t)$ is the unknown concentration at the generic node of the finite-element mesh, and N_n is the number of nodes in the mesh. The spatial and temporal partial derivatives of $\hat{c}$ are:

$$\frac{\partial \hat{c}}{\partial x_i} = \sum_{g=1}^{N_n} \frac{\partial N_g(x_1, x_2)}{\partial x_i} \cdot c_g(t) \quad ; \; i = 1, 2 \tag{12}$$

$$\frac{\partial \hat{c}}{\partial t} = \sum_{g=1}^{N_n} N_g(x_1, x_2) \cdot \frac{\partial c_g(t)}{\partial t} \tag{13}$$

Substituting Equation (11) in Equation (10) yields the residual:

$$\begin{aligned} M(\hat{c}) &= \frac{\partial}{\partial x_i}\left(D_{ij}\frac{\partial \hat{c}}{\partial x_j}\right) - v_i \cdot \frac{\partial \hat{c}}{\partial x_i} - n \cdot S_w \cdot \left(\frac{\partial \hat{c}}{\partial t} + \lambda \cdot \hat{c}\right) + \\ &- \rho_b \cdot \left[\frac{dS}{d\hat{c}} \cdot \frac{\partial \hat{c}}{\partial t} + \lambda \cdot S\left(\hat{c}\right)\right] - q \cdot (\hat{c} - c^*) + f \end{aligned} \tag{14}$$

The finite-element solution relies on the minimization of the residual (14), which is achieved by imposing its orthogonality over the domain R with N_n test functions $W_g(x_1, x_2)$. This constraint produces the weighted residual equations:

$$\int_R M(\hat{c}) \cdot W_g(x_1, x_2) \cdot dR = 0 \qquad g = 1, \ldots, N_n \tag{15}$$

Depending on the choice of the test functions W_g, different methods are formulated. For example, the classical Galerkin method assumes $W_g \equiv N_g$. In the approach followed in TRAN2D, an "upwind" Petrov-Galerkin method is implemented, where nonsymmetric test functions are used to integrate the advective component of the transport equation, whereas linear basis functions are used otherwise. This approach helps reduce numerical dispersion in advection-dominated problems [10, 14].

Since integration by parts of both the dispersive and advective components of integral (15) is known to yield unstable numerical solutions [7, 8, 9, 4] this is applied to the dispersive component only:

$$\begin{aligned} \text{(a):} \quad & -\int_R \left(D_{ij} \cdot \frac{\partial \hat{c}}{\partial x_j} \cdot \frac{\partial W_g}{\partial x_i} + v_i \cdot \frac{\partial \hat{c}}{\partial x_i} \cdot W_g\right) \cdot dR + \\ \text{(b):} \quad & +\int_\Gamma \left(D_{ij} \cdot \frac{\partial \hat{c}}{\partial x_j}\right) n_i \cdot W_g \cdot d\Gamma + \\ \text{(c):} \quad & -\int_R n \cdot S_w \cdot \left(\frac{\partial \hat{c}}{\partial t} + \lambda \hat{c}\right) \cdot W_g \cdot dR + \\ \text{(d):} \quad & -\int_R \rho_b \cdot \left[\frac{dS}{d\hat{c}} \cdot \frac{\partial \hat{c}}{\partial t} + \lambda \cdot S\left(\hat{c}\right)\right] \cdot W_g \cdot dR + \\ \text{(e):} \quad & +\int_R [(c^* - \hat{c}) \cdot q - f] \cdot W_g \cdot dR = 0 \qquad g = 1, \ldots, N_n \end{aligned} \tag{16}$$

The terms (a)-(e) in the generic Equation (16) may be expanded by substituting (11) and its partial derivatives (12) and (13), and partitioning each integral over the N_e elements of the grid. The term (b) in Equation (16) is expanded by imposing the Neumann and Cauchy

boundary conditions (6c) and (6d). These calculations are explained in the following.

$$
\begin{aligned}
\text{(a):} \qquad &= -\sum_{e=1}^{N_e}\int_{\Delta^e}\{D_{ij}^e\cdot\left[\sum_{g'=1}^{N_n}c_{g'}(t)\cdot\frac{\partial N_{g'}^e}{\partial x_j}\right]\cdot\frac{\partial W_g^e}{\partial x_i}+\\
&\quad +v_i^e\cdot\left[\sum_{g'=1}^{N_n}c_{g'}(t)\cdot\frac{\partial N_{g'}^e}{\partial x_j}\right]\cdot W_g^e\ \ \}\cdot dR^e=\\
&= -\sum_{g'=1}^{N_n}\left[\sum_{e=1}^{N_e}\int_{\Delta^e}D_{ij}^e\cdot\frac{\partial N_{g'}^e}{\partial x_j}\cdot\frac{\partial W_g^e}{\partial x_i}\cdot d\Delta^e\right]\cdot c_{g'}(t)+\\
&\quad -\sum_{g'=1}^{N_n}\left[\sum_{e=1}^{N_e}\int_{\Delta^e}v_i^e\cdot\frac{\partial N_{g'}^e}{\partial x_j}\cdot W_g^e\cdot d\Delta^e\right]\cdot c_{g'}(t)=\\
&= -\sum_{g'=1}^{N_n}A_{g,g'}\cdot c_{g'}(t)-\sum_{g'=1}^{N_n}B_{g,g'}\cdot c_{g'}(t) \qquad (17)
\end{aligned}
$$

$$
\begin{aligned}
\text{(b):} \qquad &= \int_{\Gamma_N}q_c^N(x_i,t)\cdot W_g\cdot d\Gamma_N+\\
&\quad +\int_{\Gamma_C}\left[v_i\cdot c\cdot n_i+q_c^C(x_i,t)\right]\cdot W_g\cdot d\Gamma_C=\\
&= \sum_{e=1}^{N_e}\int_{\Gamma_N^e}q_c^{Ne}(x_i,t)\cdot W_g^e\cdot d\Gamma_N^e+\\
&\quad +\sum_{g'=1}^{N_n}\left[\sum_{e=1}^{N_e}\int_{\Gamma_C^e}v_i^e\cdot n_i^e\cdot N_{g'}^e\cdot W_g^e\cdot d\Gamma_C^e\right]\cdot c_{g'}(t)\\
&+ \sum_{e=1}^{N_e}\int_{\Gamma_C^e}q_c^{Ce}\cdot W_g^e d\Gamma_C^e == r_g^N+\sum_{g'=1}^{N_n}f_{g,g'}^C\cdot c_{g'}(t)+r_g^C \qquad (18)
\end{aligned}
$$

$$
\begin{aligned}
\text{(c):} \qquad &= -\int_R n\cdot S_w\cdot\left[\sum_{g'=1}^{N_n}N_{g'}\cdot\frac{\partial c_{g'}}{\partial t}+\lambda\cdot c_{g'}(t)\right]\cdot W_g\cdot dR=\\
&= -\sum_{g'=1}^{N_n}\left[\sum_{e=1}^{N_e}\int_{\Delta^e}n^e\cdot S_w^e N_{g'}^e\cdot W_g^e\cdot d\Delta^e\right]\cdot\frac{\partial c_{g'}}{\partial t}+\\
&\quad -\sum_{g'=1}^{N_n}\left[\sum_{e=1}^{N_e}\int_{\Delta^e}n^e\cdot S_w^e\cdot\lambda^e\cdot N_{g'}^e\cdot W_g^e\cdot d\Delta^e\right]\cdot c_{g'}(t)=\\
&= -\sum_{g'=1}^{N_n}G_{g,g'}^{(1)}\cdot\frac{\partial c_{g'}}{\partial t}-\sum_{g'=1}^{N_n}E_{g,g'}\cdot c_{g'}(t) \qquad (19)
\end{aligned}
$$

$$
\begin{aligned}
\text{(d):} \qquad &= -\int_R \rho_b \cdot \left[\frac{dS}{d\hat{c}} \cdot \sum_{g'=1}^{N_n} N_{g'} \cdot \frac{\partial c_{g'}}{\partial t} + \lambda \cdot S(\hat{c}) \right] \cdot W_g \cdot dR = \\
&= -\sum_{e=1}^{N_e} \int_{\Delta^e} \rho_b^e \cdot \left[\frac{dS^e}{d\hat{c}} \cdot \sum_{g'=1}^{N_n} N_{g'}^e \cdot \frac{\partial c_{g'}}{\partial t} + \lambda^e \cdot S^e(\hat{c}) \right] \cdot W_g^e \cdot d\Delta^e = \\
&= -\sum_{g'=1}^{N_n} \left[\sum_{e=1}^{N_e} \int_{\Delta^e} \rho_b^e \cdot \frac{dS^e}{d\hat{c}} \cdot N_{g'}^e \cdot W_g^e \cdot d\Delta^e \right] \cdot \frac{\partial c_{g'}}{\partial t} + \\
&\quad -\sum_{e=1}^{N_e} \int_{\Delta^e} \rho_b^e \cdot \lambda^e \cdot S^e(\hat{c}) \cdot W_g^e \cdot d\Delta^e = \\
&= -\sum_{g'=1}^{N_n} G_{g,g'}^{(2)}(\hat{c}) \cdot \frac{\partial c_{g'}}{\partial t} - d_g(\hat{c}) \qquad (20)
\end{aligned}
$$

$$
\begin{aligned}
\text{(e):} \qquad &= -\int_R \left[\left(\sum_{g'=1}^{N_n} N_{g'} \cdot c'_g(t) - c^* \right) \cdot q - f \right] \cdot W_g \cdot dR = \\
&= -\sum_{e=1}^{N_e} \int_{\Delta^e} \left[\left(\sum_{g'=1}^{N_n} N_{g'}^e \cdot c'_g(t) - c^* \right) \cdot q^e - f^e \right] \cdot W_g^e \cdot d\Delta^e = \\
&= -\sum_{g'=1}^{N_n} \left[\sum_{e=1}^{N_e} \int_{\Delta^e} N_{g'}^e \cdot W_g^e \cdot q^e \cdot d\Delta^e \right] \cdot c'_g(t) + \\
&\quad + \sum_{e=1}^{N_e} \int_{\Delta^e} (q^e \cdot c^* + f^e) \cdot W_g^e \cdot d\Delta^e = \\
&= -\sum_{g'=1}^{N_n} f_{g,g'}^F \cdot c_{g'}(t) + r_g^F \qquad (21)
\end{aligned}
$$

Substituting Equations (17)-(21) into Equation (16) gives:

$$
\begin{aligned}
&\sum_{g'=1}^{N_n} \left[A_{g,g'} + B_{g,g'} - f_{g,g'}^C + E_{g,g'} + f_{g,g'}^F \right] \cdot c_{g'}(t) + \\
+ \quad &\sum_{g'=1}^{N_n} \left[G_{g,g'}^{(1)} + G_{g,g'}^{(2)}(\hat{c}) \right] \cdot \frac{\partial c_{g'}}{\partial t} - r_g^N - r_g^C + d_g(\hat{c}) - r_g^F = 0 \qquad (22) \\
&g = 1, \ldots, N_n
\end{aligned}
$$

where:

$$
A_{g,g'} = \sum_{e=1}^{N_e} \int_{\Delta^e} D_{ij}^e \cdot \frac{\partial N_{g'}^e}{\partial x_j} \cdot \frac{\partial W_g^e}{\partial x_i} \cdot d\Delta^e
$$

$$
B_{g,g'} = \sum_{e=1}^{N_e} \int_{\Delta^e} v_i^e \cdot \frac{\partial N_{g'}^e}{\partial x_i} \cdot W_g^e \cdot d\Delta^e
$$

$$
\begin{aligned}
E_{g,g'} &= \sum_{e=1}^{N_e} \int_{\Delta^e} n^e \cdot S_w^e \cdot \lambda^e \cdot N_{g'}^e \cdot W_g^e \cdot d\Delta^e \\
F_{g,g'} &= f_{g,g'}^F - f_{g,g'}^C = \sum_{e=1}^{N_e} \int_{\Delta^e} q^e \cdot N_{g'}^e \cdot W_g^e \cdot d\Delta^e + \\
&\quad - \sum_{e=1}^{N_e} \int_{\Gamma_C^e} (v_i^e \cdot n_i^e) \cdot N_{g'}^e \cdot W_g^e \cdot d\Gamma_C^e \\
G_{g,g'}(\hat{c}) &= G_{g,g'}^{(1)} + G_{g,g'}^{(2)}(\hat{c}) = \sum_{e=1}^{N_e} \int_{\Delta^e} n^e \cdot S_w^e \cdot N_{g'}^e \cdot W_g^e \cdot d\Delta^e + \\
&\quad + \sum_{e=1}^{N_e} \int_{\Delta^e} \rho_b^e \cdot \frac{dS^e}{d\hat{c}} \cdot N_{g'}^e \cdot W_g^e \cdot d\Delta^e \qquad (23) \\
R_g(\hat{c}) &= -r_g^F - r_g^N - r_g^C + d_g(\hat{c}) = -\sum_{e=1}^{N_e} \int_{\Delta^e} (q^e c^{*^e} + f^e) \cdot W_g^e \cdot d\Delta^e + \\
&\quad - \sum_{e=1}^{N_e} \int_{\Gamma_N^e} q_c^{N^e} \cdot W_g^e \cdot d\Gamma_N^e - \sum_{e=1}^{N_e} \int_{\Gamma_C^e} q_c^{C^e} \cdot W_g^e \cdot d\Gamma_C^e + \\
&\quad + \sum_{e=1}^{N_e} \int_{\Delta^e} \rho_b^e \cdot \lambda^e \cdot S^e(\hat{c}) \cdot W_g^e \cdot d\Delta^e \qquad (24)
\end{aligned}
$$

It is worth noting that the generic Equation (22) is non-linear as the two terms (23) and (24), which include the sorption isotherm and its derivative, are concentration-dependent. Equations (22) represent a system of N_n non-linear equations for the unknown nodal concentrations $\boldsymbol{c} = (c_1, c_2, \ldots, c_{N_n})^T$:

$$
[\boldsymbol{A} + \boldsymbol{B} + \boldsymbol{E} + \boldsymbol{F}] \cdot \boldsymbol{c} + \boldsymbol{G}(\boldsymbol{c}) \cdot \frac{\partial \boldsymbol{c}}{\partial t} + \boldsymbol{R}(\boldsymbol{c}) = \boldsymbol{0} \qquad (25)
$$

Integration in time of Equation (25) is performed using a weighted finite-difference scheme:

$$
\begin{aligned}
\boldsymbol{c} &= \nu \cdot \boldsymbol{c}_{(k+1)} + (1-\nu) \cdot \boldsymbol{c}_{(k)} \qquad (26) \\
\frac{\partial \boldsymbol{c}}{\partial t} &= \frac{\boldsymbol{c}_{(k+1)} - \boldsymbol{c}_{(k)}}{t_{(k+1)} - t_{(k)}} = \frac{\boldsymbol{c}_{(k+1)} - \boldsymbol{c}_{(k)}}{\Delta t_k} \qquad (27)
\end{aligned}
$$

After introducing Equations (26) and (27) into (25), the following finite-difference scheme is obtained:

$$
\begin{aligned}
&\{\nu \cdot [\boldsymbol{A} + \boldsymbol{B} + \boldsymbol{E} + \boldsymbol{F}]_{(k+\nu)} + \frac{1}{\Delta t_k} \cdot \boldsymbol{G}(\boldsymbol{c})_{(k+\nu)}\} \cdot \boldsymbol{c}_{(k+1)} = \\
= \ &\{\frac{1}{\Delta t_k} \cdot \boldsymbol{G}(\boldsymbol{c})_{(k+\nu)} - (1-\nu) \cdot [\boldsymbol{A} + \boldsymbol{B} + \boldsymbol{E} + \boldsymbol{F}]_{(k+\nu)}\} \cdot \boldsymbol{c}_k - \boldsymbol{R}(\boldsymbol{c})_{(k+\nu)}
\end{aligned} \qquad (28)
$$

Scheme (28) is sensitive to the value of the weighting parameter ν: ν values close to $1/2$ lead to accurate but unstable solutions, while ν values close to 1 yield good stability but large numerical dispersion [12].

To address the non linearity of the system (28), a Picard iteration procedure is here proposed:

$$\begin{aligned} & \{\nu \cdot [\boldsymbol{A}+\boldsymbol{B}+\boldsymbol{E}+\boldsymbol{F}]_{(k+\nu)} + \frac{1}{\Delta t_k} \cdot \boldsymbol{G}\left[\boldsymbol{c}^m_{(k+\nu)}\right]\} \cdot \boldsymbol{c}^{m+1}_{(k+1)} = \\ = \; & \{\frac{1}{\Delta t_k}\boldsymbol{G}(\boldsymbol{c}^m_{(k+\nu)}) - (1-\nu) \cdot [\boldsymbol{A}+\boldsymbol{B}+\boldsymbol{E}+\boldsymbol{F}]_{(k+\nu)}\} \cdot \boldsymbol{c}_{(k)} - \boldsymbol{R}\left[\boldsymbol{c}^m_{(k+\nu)}\right] \end{aligned} \tag{29}$$

where m is the Picard iteration index. At each time step, the linear set of equations (29) is solved repeatedly until the concentration vector $\boldsymbol{c}^{m+1}_{(k+1)}$ reaches convergence. $\boldsymbol{c}^{m+1}_{(k+1)}$ is then used as initial guess for the concentration distribution at the following time step. In scheme (29), the evaluation of the matrices that do not depend on concentration (that is, $\boldsymbol{A}$, $\boldsymbol{B}$, $\boldsymbol{E}$, and $\boldsymbol{F}$) is performed using the values of velocity and water saturation at time level $k+\nu$ calculated by solving the Richard's equation. The concentration dependent terms (that is, $\boldsymbol{G}$ and $\boldsymbol{R}$) are updated at each iteration m based upon a weighted average concentration calculated as in Equation (26). At each iteration, Dirichlet boundary conditions (6a) are imposed after the discretized system has been assembled. This is carried out by modifying the rows of the system (29) corresponding to the Dirichlet nodes: (i) extra-diagonal coefficients are set equal to zero; (ii) the diagonal coefficient is set equal to one; (iii) the known term is set equal to the Dirichlet boundary solute concentration.

5 Solute Mass balance

At the end of each time step, the accuracy of the finite-element solution may be assessed by calculating the terms of the solute mass balance equation, and checking whether the difference between inflows and outflows is equal the variation in the mass of solute stored in the system. The mass balance relies upon the integration of Equation (5) over the domain R. In the finite-element formulation presented here, the mass balance equation for the current time step Δt_k may be written as:

$$M_{D(k+1)} + M_{N(k+1)} + M_{C(k+1)} + M_{F(k+1)} = \Delta M_{(k+1)} \tag{30}$$

where: $M_{D(k+1)}$, $M_{N(k+1)}$, and $M_{C(k+1)}$ are the net solute masses exchanged through the Dirichlet, Neumann, and Cauchy boundaries, respectively; $M_{F(k+1)}$ is the net solute mass entering the system associated with the source term $(q \cdot c^* + f)$ (Equation (1)); and $\Delta M_{(k+1)}$ is the change in the solute mass stored in the domain. The masses $M_{D(k+1)}$, $M_{N(k+1)}$, and $M_{C(k+1)}$ may be calculated as:

$$\begin{aligned} M_{D(k+1)} &= \{\int_{\Gamma_D} q^D_{c(k+\nu)} \cdot d\Gamma_D\} \cdot \Delta t_k \\ M_{N(k+1)} &= \{\int_{\Gamma_N} q^N_{c(k+\nu)} \cdot d\Gamma_N\} \cdot \Delta t_k \\ M_{C(k+1)} &= \{\int_{\Gamma_C} q^C_{c(k+\nu)} \cdot d\Gamma_C\} \cdot \Delta t_k \\ M_{F(k+1)} &= \{\int_{R} (q \cdot c^* + f)_{(k+\nu)} \cdot dR\} \cdot \Delta t_k \end{aligned}$$

where the subscript $(k+\nu)$ represent the weighted average calculated in a fashion analogous to Equation (26).

After the iterative scheme (29) has converged, the solute mass rates exchanged through the nodes of the Dirichlet, Neumann, and Cauchy boundaries may be obtained from the matrix-vector product at the right-hand side of Equation (29) calculated using the matrix coefficients prior to imposing the Dirichlet boundary conditions. In practice, these mass rates allow for the calculation of $M_{D(k+1)}$, $M_{N(k+1)}$, $M_{C(k+1)}$ and $M_{F(k+1)}$. The change in the solute mass stored in the domain during the time step Δt_k may be estimated as:

$$\begin{aligned} \Delta M_{(k+1)} &= \sum_{e=1}^{N_e} \int_{\Delta^e} \{ n^e \cdot S_w^e \left[\hat{c}_{(k+1)} - \hat{c}_{(k)} + \lambda^e \cdot \hat{c}_{(k+\nu)} \right] + \\ &+ \rho_b^e \cdot \left[S^e(\hat{c}_{(k+1)}) - S^e(\hat{c}_{(k)}) + \lambda^e \cdot S^e(\hat{c}_{(k+\nu)}) \right] \} \cdot d\Delta^e \end{aligned} \tag{31}$$

The absolute mass balance error is thus given by:

$$\epsilon_a = \mid M_{D(k+1)} + M_{N(k+1)} + M_{C(k+1)} + M_{F(k+1)} - \Delta M_{(k+1)} \mid \tag{32}$$

The relative mass balance error may be calculated as:

$$\epsilon_r = \frac{2 \cdot \epsilon_a}{\mid M_{D(k+1)} + M_{N(k+1)} + M_{C(k+1)} + M_{F(k+1)} + \Delta M_{(k+1)} \mid} \tag{33}$$

6 Test Simulations

Analytical solutions for a tracer in a semi-infinite one-dimensional (1-D) homogeneous domain undergoing radioactive decay and linear equilibrium sorption may be found in [1]. In this domain, flow is assumed to be at steady-state and uniform. The initial condition is $c(x,0) = 0$, whereas boundary conditions are $c(0,t) = c_0$ and $c\,(x \to \infty, t) = 0$. These solutions are here used to test the accuracy of the simulation results obtained with TRAN2D.NLS. In this set of simulations, use is made of the hydrogeological parameters presented in Table 1.

Table 1: Test Case: hydrogeological parameters

Porosity	n (/)	0.3
Water Saturation	S_w (/)	1.0
Solid Density	ρ_s (kg/m^3)	2650
Darcy Velocity	v (m/s)	1.0×10^{-7}
Boundary Concentration	c_0 (kg/m^3)	1.0
Molecular Diffusivity	D_o (m^2/s)	6.6×10^{-6}
Tortuosity	τ (/)	0.4
Longitudinal Dispersivity	α_L (m)	10.0
Decay Rate Constant	λ (s^{-1})	4.40×10^{-9}
Distribution Coefficient	K_F (m^3/kg)	1.66×10^{-3}
Adsorption Constant	K_L (m^3/kg)	1.66×10^{-3}
Sorption Capacity	S_{lim} (kg/kg)	1.66×10^{-4}

To represent the semi-infinite 1-D column, a 2×200 (m×m) rectangular domain is discretized with the finite-element mesh shown in Figure 2. At the left and right boundaries of the domain, the two Dirichlet conditions $c(0,t) = c_0$ and $c(200$ m,$t) = 0$ are imposed,

respectively. The upper and lower longitudinal edges are considered Neumann boundaries, where the dispersive flux q_c^N is set to zero. The longitudinal size of the grid is large enough to ensure that the breaktrough profiles at the time of interest are not affected by the downstream boundary condition. The resolution of this grid is chosen in order to prevent effects of numerical dispersio, which are expected to occur when the element size is of the same order of the longitudinal dispersivity. In the simulation tests, a time step Δt= 1 day is adopted.

Figure 3 shows the solute concentration profiles obtained at time t=1825 days in the case of a conservative solute (λ=0; K_F=0) using both the analytical solution (see Equation (7-134) in Bear [1]) and the numerical model TRAN2D.NLS. The numerical results closely match the analytical model.

Figure 4 shows the analytical and the numerical solute concentration profiles obtained at time t=1825 days in the case of a solute undergoing decay(λ=4.40$\times 10^{-9}$s^{-1}; K_F=0).The analytical breakthrough curve (see Equation (7-133) in Bear [1]) is accurately reproduced by the numerical model.

Figure 5 displays the solute concentration distributions at time t=1825 days in the case of a solute undergoing linear sorption (λ=0; K_F=1.66$\times 10^{-3}$ m^3/kg; N=1) obtained using the analytical solution (see Equation (7-135) in Bear [1]) and the numerical model TRAN2D.NLS. Even in this case, the numerical results coincide with the analytical solution.

Figure 6 shows the solute concentration profiles at time t=1825 days obtained assuming a non-linear Freundlich isotherm with N values equal to 0.8 and 1.25, and a linear soprtion isotherm (N=1). In each case the same value of the distribution coefficient K_F is considered. Note that, because of the non-linear nature of the isotherms, no analytical solution is available, therefore the numerical approach implemented in TRAN2D.NLS is necessary to simulate the behavior of the contaminant front. It may be observed that if N is greater than 1 the breakthrough curve is spreading, while it is self-sharpening if N is less than 1. A similar observation is made by Fetter [3].

Figure 7 compare the breakthrough profiles at time t=1825 days obtained assuming, in one case, a linear sorption isotherm with K_F=1.66$\times 10^{-3}$ m^3/kg, and, in another a non-linear Langmuir isotherm with K_L=1.66$\times 10^{-3}$ m^3/kg and S_{lim}=1.66$\times 10^{-4}$ (kg/kg). It is evident that, because of the limited sorption capacity that may be accounted for, with the Langmuir model the solute concentration results significantly higher than that predicted using the linear isotherm.

Figures 8 shows the convergence profiles for the Picard iteration implemented in TRAN2D.NLS, obtained at the 20^{th} time step using different values of the non-linear sorption isotherm parameters. These profiles represent the maximum change in the concentration distribution that is calculated at each iteration in the Picard scheme (Equation (29)) plotted against the iteration index m.

Figure 8a refers to Freundlich isotherms with K_F=1.66$\times 10^{-3}$ m^3/kg and increasing values

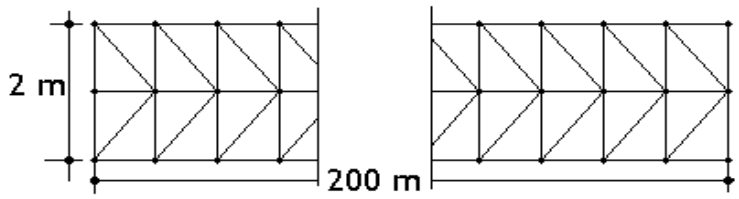

Figure 2: Detail of the finite-element mesh, characterized by 603 nodes and 800 triangular elements.

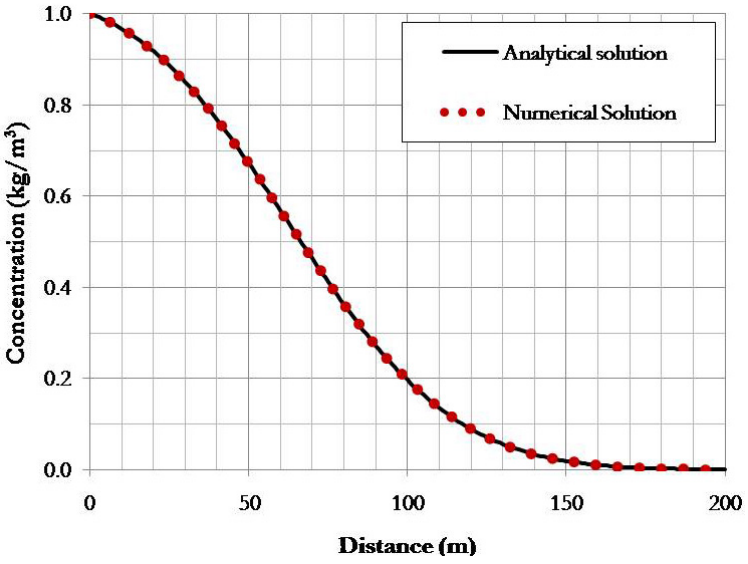

Figure 3: Comparison between the numerical and analytical solutions obtained assuming the solute as conservative (λ=0; K_F=0).

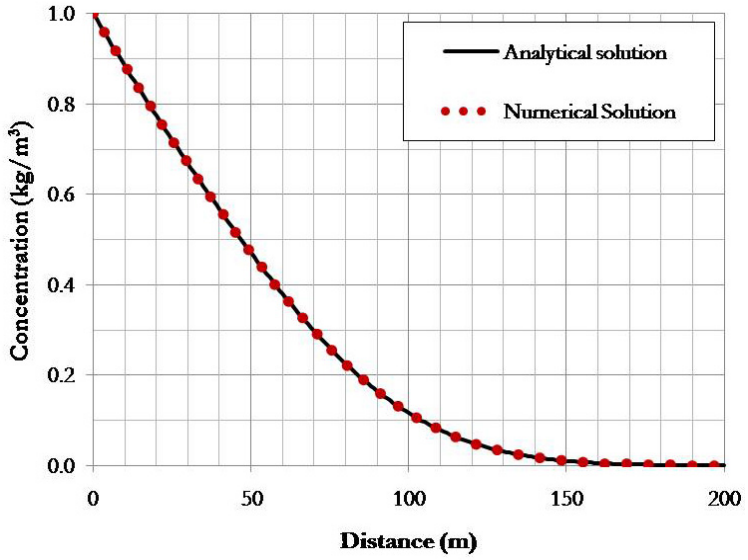

Figure 4: Comparison between the numerical and analytical solutions obtained assuming the solute as decaying with λ=4.40×10^{-9}s^{-1}.

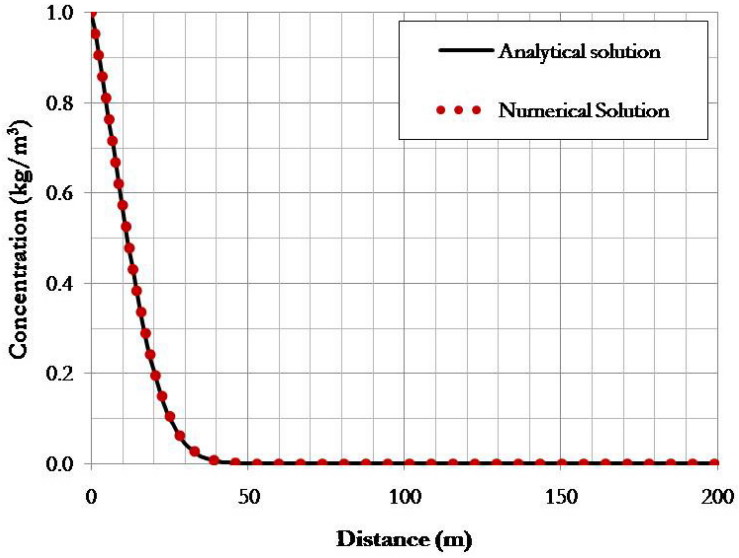

Figure 5: Comparison between the numerical and analytical solutions obtained assuming the solute undergoes linear sorption (K_F=1.66×10^{-3} m^3/kg; N=1).

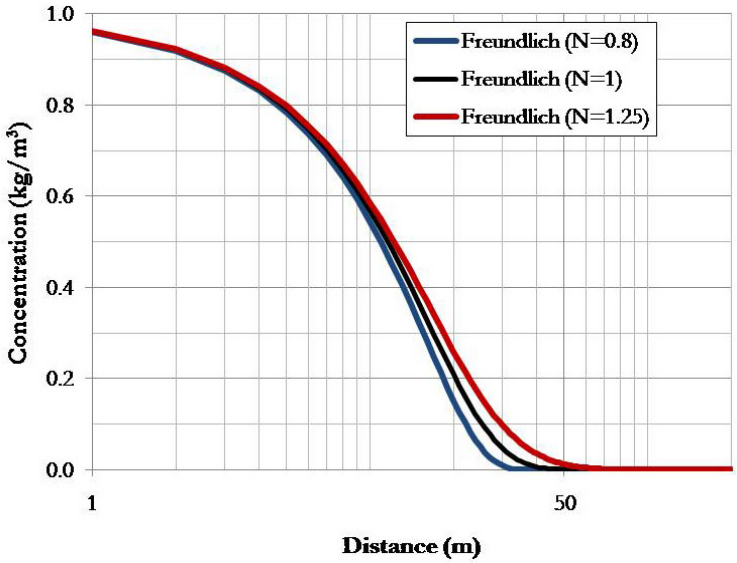

Figure 6: Comparison between the numerical solutions obtained assuming Freundlich non-linear sorption isotherms with different N values (λ=0 ; K_F=1.66×10^{-3} m^3/kg).

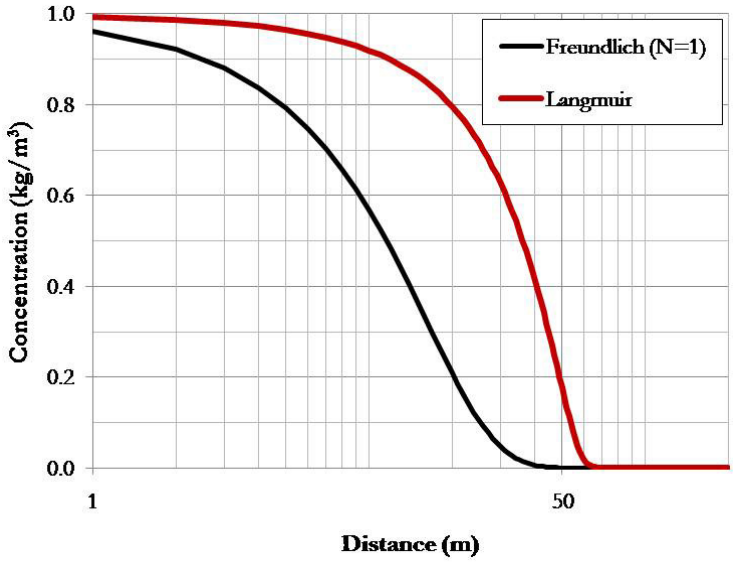

Figure 7: Comparison between the numerical solutions obtained assuming in one case a Freundlich linear isotherm (K_F=1.66×10^{-3} m^3/kg; N=1) and a rate-limited Langmuir isotherm (K_L=1.66×10^{-3} m^3/kg); S_{lim}=1.66×10^{-4} (kg/kg) in another.

of N. It is observed that the convergence rate is approximately log-linear, and is lower for either small or large values of the coefficient N. On the other hand, if N approaches 1, the isotherm tends to be linear and convergence is faster. If N=1, convergence is achieved with one single iteration (m=1).

Figure 8b refers to Langmuir isotherms with K_L=1.66×10^{-3} m^3/kg and values of S_{lim} increasing from 1×10^{-4} to 1.66×10^{-3} kg/m^3. Even in this case, the convergence rate is approximately log-linear, and is lower for low values of S_{lim}. In practice, the Langmuir isotherm may be modeled as a simple linear isotherm if the sorption capacity is significantly larger than the product between K_L and the concentration of the contaminant source.

7 Conclusions

Finite element models can be effectively used to study the migration and fate of contaminants dissolved in groundwater in realistically heterogeneous scenarios. These models rely on the solution by variational methods to the partial differential equations that express the mass continuity for the aquifer/contaminant system. In this work, a two-dimensional finite-element model has been developed to simulate groundwater transport of a solute undergoing advection, dispersion, first-order decay, and non-linear local-equilibrium sorption. The model applies to real-world applications in which sorption rates are much faster than the rates of advection and dispersion. The model can deal with common non-linear sorption models, such as Freundlich's or Langmuir's, as well as arbitrary isotherms specified using piecewise linear functions. To tackle the non linearity introduced in the transport equation by non linear isotherms, a direct iterative approach was devised based upon a straighforward Picard linearization. The transport model was benchmarked against analytical solutions available in the literature for highly idealized one-dimensional settings. The model was then used in a number of preliminary tests, where no analytical solutions are available, which were de-

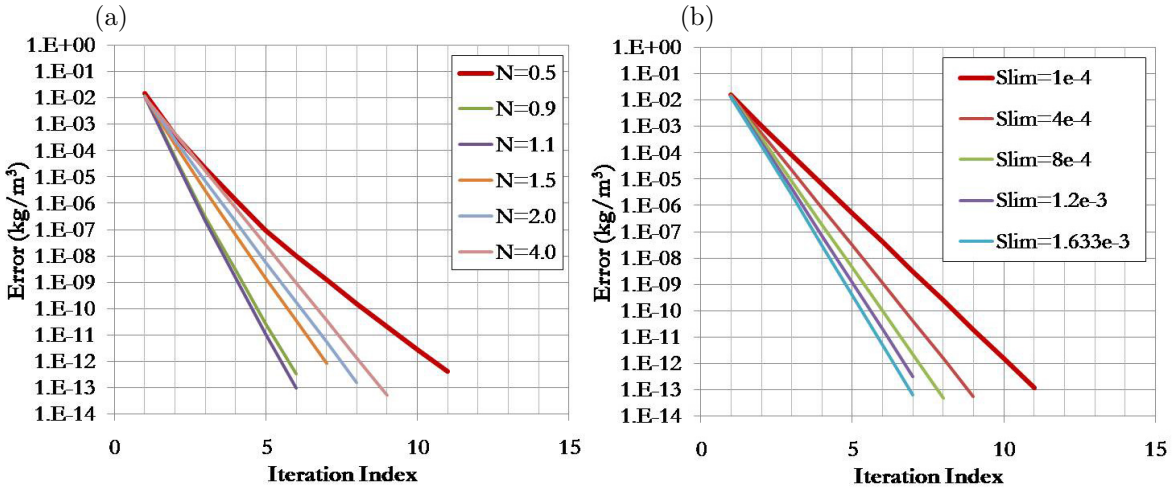

Figure 8: Convergence profiles obtained using increasing values of the (a) Freundlich and (b) Langmuir sorption isotherm parameters.

veloped to: (a) study the sorption effects as simulated using different non-linear isotherm models; (b) verify the computational efficiency of the devised Picard iterative scheme.

Acknowledgements. The author is very grateful to Dr. Mario Putti, from the University of Padua, Italy, for his valuable comments and suggestions and for the gracious use of the numerical contaminant transport model TRAN2D, which was modified to the develop the code TRAN2D.NLS presented here.

References

[1] Bear, J. (1979). *Hydraulics of Groundwater*. McGraw-Hill, New York.

[2] Brusseau, M. L. and Rao, P. S. C. (1989). Sorption nonideality during organic contaminant transport in porous media. *Crit. Rev. Env. Contr.*, **19(1)**, 33–99.

[3] Fetter, C. W. (1999). *Contaminant Hydrogeology*. Clarendon Press, Prentice-Hall, 2nd edition.

[4] Galeati, G. and Gambolati, G. (1989). On boundary conditions and point sources in the finite element integration of the transport equation. *Water Resour. Res.*, **25**(5), 847–856.

[5] Gambolati, G., Paniconi, C., and Putti, M. (1993). Numerical modeling of contaminant transport in groundwater. In D. Petruzzelli and F. G. Helfferich, editors, *Migration and Fate of Pollutants in Soils and Subsoils*, volume 32 of *NATO ASI Series G: Ecological Sciences*, pages 381–410, Berlin. Springer-Verlag.

[6] Gambolati, G., Pini, G., Putti, M., and Paniconi, C. (1994). Finite element modeling of the transport of reactive contaminants in variably saturated soils with LEA and non-LEA sorption. In P. Zannetti, editor, *Environmental Modeling, Vol. II: Computer Methods and Software for Simulating Environmental Pollution and its Adverse Effects*, chapter 7, pages 173–212. Computational Mechanics Publications, Southampton, UK.

[7] Gureghian, A. B. (1983). TRIPM, a two-dimensional finite element model for the simultaneous transport of water and reacting solutes through saturated and unsaturated porous media. Technical Report ONWI-465, Off. of Nuclear Water Isolation, Columbus, Ohio.

[8] Huyakorn, P. S. and Pinder, G. F. (1983). *Computational Methods in Subsurface Flow*. Academic Press, London.

[9] Huyakorn, P. S., Mercer, J. W., and Ward, D. S. (1985). Finite element matrix and mass balance computational schemes for transport in variably saturated porous media. *Water Resour. Res.*, **21**(3), 346–358.

[10] Huyakorn, P. S., Andersen, P. F., Mercer, J. W., and White, H. O. (1987). Saltwater intrusion in aquifers: Development and testing of a three-dimensional finite element model. *Water Resour. Res.*, **23**(2), 293–312.

[11] Nielsen, D. R., van Genuchten, M. T., and Biggar, A. J. W. (1986). Water flow and solute transport processes in the unsaturated zone. *Water Resour. Res.*, **22**(9), 89S–108S.

[12] Peyret, R. and Taylor, T. D. (1983). *Computational Methods for Fluid Flow*. Springer-Verlag, New York.

[13] Philip, J. R. (1969). Theory of infiltration. *Adv. Hydrosci.*, **5**, 215–296.

[14] Pini, G., Gambolati, G., and Galeati, G. (1989). 3-D finite element transport models by upwind preconditioned conjugate gradients. *Adv. Water Resources*, **12**, 54–58.

[15] Weber Jr., W. J., McGinley, P., and Katz, L. (1991). Sorption phenomena in subsurface systems: Concepts, models and effects on contaminant fate and transport. *Water Res.*, **25**(5), 499–528.